



REVIEW

Alexander Ricker  · Nils Hendrik Kröger · Peter Wriggers

Comparison of discontinuous damage models of Mullins-type

Received: 31 March 2021 / Accepted: 21 July 2021
© The Author(s), corrected publication 2021

Abstract The Mullins effect is a characteristic property of filled rubber materials whose accurate and efficient modelling is still a challenging task. Innumerable constitutive models for elastomers are described in the literature. Therefore, this contribution gives a review on some widely used approaches, presents a classification, proves their thermodynamic consistency, and discusses reasonable modifications. To reduce the wide range of models, the choice is restricted to those which reproduce the idealised, discontinuous Mullins effect. Apart from the theoretical considerations, two compounds were produced and tested under cyclic uniaxial and equibiaxial tension as well as pure shear. Based on this experimental data, a benchmark that compares the fitting quality of the discussed models is compiled and favourable approaches are identified. The results are a sound basis for establishing novel or improving existing rubber models.

Keywords Rubber materials · Experimental validation · Material modeling · Mullins effect

1 Introduction

Many modelling approaches in finite strain continuum mechanics are motivated by the complex behaviour of polymers. In particular, reproducing the characteristic stress response of elastomers—including strong nonlinearity, permanent set, equilibrium hysteresis, material softening (also known as Mullins effect), rate and temperature dependence—is a challenging task. Earliest constitutive models for rubber materials which are suitable for large deformation and three-dimensional analyses date back to the 1940s, cf. Mooney-Rivlin and Neo-Hooke model. Since then, many authors invested in more realistic and sophisticated models, see [6] for an overview. Though, to the best of our knowledge, no existing model is able to capture all these effects accurately and efficiently in a thermodynamically consistent and numerically robust way. However, a promising attempt is made for example by [35].

This paper takes a step back and focuses on models that reproduce damage according to the idealised Mullins effect. *Idealised* denotes, that these models consider neither permanent set nor equilibrium hysteresis. Moreover, only discontinuous softening is reproduced, see Fig. 1. Of course, this is a strong simplification such that these models are not sufficient to reproduce all material effects discussed above without further effort.

A. Ricker (✉) · P. Wriggers
Institute of Continuum Mechanics, Leibniz Universität Hannover, An der Universität 1, 30823 Garbsen, Germany

A. Ricker
Department Simulation and Continuum Mechanics, Deutsches Institut für Kautschuktechnologie e.V., Eupener Straße 33, 30519 Hannover, Germany
E-mail: alexander.ricker@ikm.uni-hannover.de

N. H. Kröger
material prediction GmbH, Nordkamp 14, 26203 Wardenburg, Germany

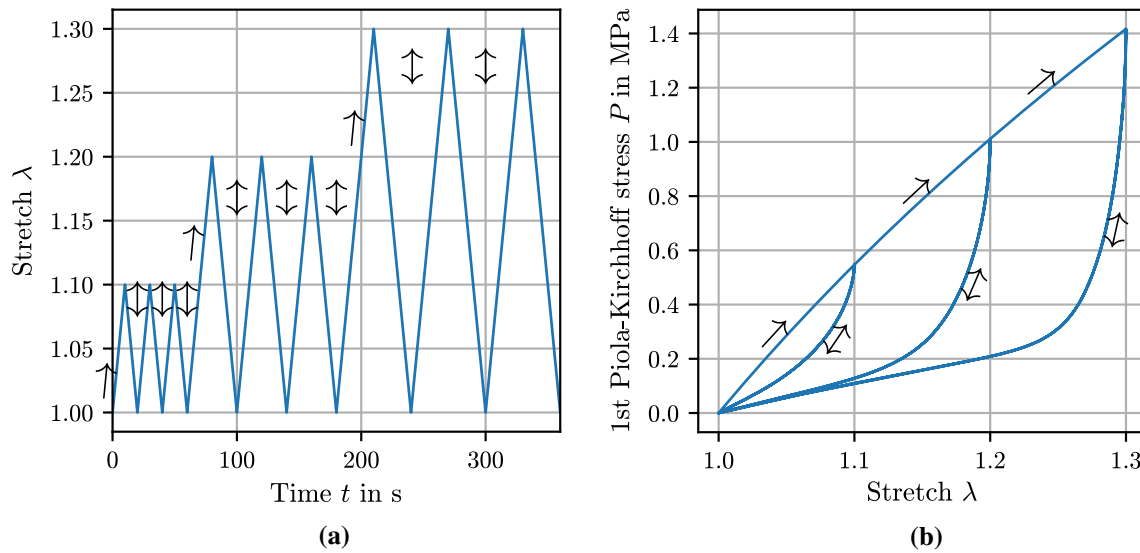


Fig. 1 Idealised Mullins effect: **a** cyclic input data, **b** stress response according to the idealised Mullins effect (\rightarrow and \leftrightarrow denote the virgin loading and un-/reloading, respectively)

Instead, these models should be considered as a starting point of more complex approaches. For instance, [4] proposed a model based on such an idealised softening and added a rate-independent, plastic contribution which generates equilibrium hysteresis and permanent set. Also the derivation of the elastoplastic model by [27] which was extended to viscoelastoplasticity by [36] starts from an idealised softening. Further, [19] presented a viscoelastic model whose equilibrium stress is affected by idealised softening.

In spite of the limitations, Mullins-type damage models on their own are a reliable alternative for approximating the behaviour of filled rubber in certain applications. Since the choice of models is always a trade-off between numerical effort and the realism of their behaviour, the simulation purpose must be kept in mind. Here, a good prediction of the structural stiffness depending on the maximum load the material has experienced so far can be obtained. For instance, the structural stiffness is of crucial importance for damping components that either experience softening in use or are prestretched within the production process. Another example are seals whose closing pressure may be affected by the material softening. Moreover, the static behaviour after cyclic loading, e.g., interrupted fatigue tests can be estimated by damage models.

The present paper conducts a benchmark of the aforementioned damage models. Lists or rankings of rubber models have indeed been compiled in the recent years for example by [10], [28] or [39]. However, these publications deal with purely elastic models only. Looking for more sophisticated models, comparative reviews typically deal with two or three particular models only. For example, [17] compared only two damage approaches each combined with the polynomial strain energy function by [43]. In contrast, this paper pursues a more general comparison and takes fifteen approaches into account. In addition, four modifications are presented and included in the comparison.

Aiming for the best fit quality, each approach is tested with several hyperelastic models, see Sect. 3.1. Therefore, discontinuous damage models that can be added to an arbitrary, isotropic hyperelastic strain energy function Ψ_0 suitable for large deformations are taken into account. Moreover, models with increased numerical effort, e.g., numerical integration, sums over material/chain directions, numerical methods for differential equations or split of the deformation gradient which separates the damage kinematics are excluded. Finally, we restrict ourselves to isochoric damage since experimental findings indicate that the volumetric part can be treated as nearly perfectly elastic, see for example [16] or [37]. Summing up, this contribution aims for a comparison and discussion of numerical efficient, generalisable, isotropic, discontinuous modelling approaches for isochoric Mullins-type damage.

The paper is organised as follows: Sect. 2 provides the required basics and thermodynamics of damage models as well as an introduction to the fitting procedure. The theories and constitutive equations of the damage models and the basic hyperelastic models are briefly summed up in Sect. 3. After describing the experimental procedure in Sect. 4, the results are discussed in detail in Sect. 5.

2 General considerations

2.1 Basic kinematics

Considering a material point with the position vector \mathbf{X} in the reference configuration and position vector \mathbf{x} in the current configuration, the according deformation gradient and the right Cauchy-Green tensor are given by

$$\mathbf{F} = \frac{\partial \mathbf{x}}{\partial \mathbf{X}} \quad \text{and} \quad \mathbf{C} = \mathbf{F}^T \cdot \mathbf{F}, \quad (1)$$

respectively, where \mathbf{F}^T is the transposed deformation gradient. The square-root of the eigenvalues of \mathbf{C} are called principal stretches and are denoted by λ_x , λ_y and λ_z . However, the deformation can be multiplicatively decomposed into a volumetric and an isochoric part

$$\begin{aligned} \hat{\mathbf{F}} &= J^{\frac{1}{3}} \mathbf{I} \quad \text{with} \quad J = \det(\mathbf{F}) \quad \text{and} \\ \bar{\mathbf{F}} &= \frac{\mathbf{F}}{J^{\frac{1}{3}}} \quad \text{with} \quad \det(\bar{\mathbf{F}}) = 1, \end{aligned} \quad (2)$$

respectively, where \mathbf{I} and $\det(\cdot)$ denote the unit tensor and the determinant. The isochoric right Cauchy-Green tensor and its principal invariants are defined as

$$\bar{\mathbf{C}} = \bar{\mathbf{F}}^T \cdot \bar{\mathbf{F}} \quad \text{and} \quad \bar{I}_1 = \text{tr}(\bar{\mathbf{C}}), \quad \bar{I}_2 = \text{tr}(\bar{\mathbf{C}}^{-1}) \quad (3)$$

with the inverse isochoric right Cauchy-Green tensor $\bar{\mathbf{C}}^{-1}$ and the trace $\text{tr}(\cdot)$. Accordingly, the square-root of the eigenvalues of $\bar{\mathbf{C}}$ are called isochoric stretches $\bar{\lambda}_x$, $\bar{\lambda}_y$ and $\bar{\lambda}_z$.

2.2 Thermodynamics

The local, isothermal Clausius-Planck inequality per unit reference volume in terms of the Helmholtz free energy density¹ is given by

$$\mathcal{D}_m = \frac{1}{2} \mathbf{S} : \dot{\mathbf{C}} - \dot{\Psi} \geq 0 \quad (4)$$

with $\mathbf{S} : \dot{\mathbf{C}} = S_{ab} \dot{C}_{ab}$ (sum over a and b), see for instance [18]. Basically, this inequality demands that for thermodynamic consistency the dissipation rate \mathcal{D}_m must be non-negative at any deformation state. \mathcal{D}_m is equal to the mechanical stress power $\frac{1}{2} \mathbf{S} : \dot{\mathbf{C}}$ less the change of the free energy $\dot{\Psi}$. Herein, \mathbf{S} denotes the 2nd Piola-Kirchhoff stress and $\dot{\mathbf{C}}$ the material time derivative of \mathbf{C} .

Assuming the free energy to be a function of \mathbf{C} and a scalar history variable Γ , the derivative of the free energy with respect to time reads $\dot{\Psi} = \frac{\partial \Psi}{\partial \mathbf{C}} : \dot{\mathbf{C}} + \frac{\partial \Psi}{\partial \Gamma} \dot{\Gamma}$ leading to

$$\mathcal{D}_m = \left(\frac{1}{2} \mathbf{S} - \frac{\partial \Psi}{\partial \mathbf{C}} \right) : \dot{\mathbf{C}} - \frac{\partial \Psi}{\partial \Gamma} \dot{\Gamma} \geq 0. \quad (5)$$

Following the standard argumentation of [9], this inequality can be fulfilled for arbitrary deformations by defining

$$\mathbf{S} = 2 \frac{\partial \Psi}{\partial \mathbf{C}} \quad (6)$$

and ensuring

$$\mathcal{D}_m = - \frac{\partial \Psi}{\partial \Gamma} \dot{\Gamma} \geq 0. \quad (7)$$

Equation (6) defines the 2nd Piola-Kirchhoff stress, whereas Eq. (7) is a restriction on the damage model.

¹ For the sake of readability, the Helmholtz free energy density is briefly referred to as free energy.

The idealised Mullins effect is commonly modelled by introducing a scalar measure of the maximum load Γ as a history variable. This measure is typically chosen to be an invariant of a deformation tensor or the basic strain energy itself. Moreover, all considered models introduce an internal state variable whose evolution is a function of this measure. Depending on the type of the internal state variable, the models may be classified into three groups: models with

1. a virgin state variable η ,
2. a damage variable d ,
3. an amplification variable X .

However, as we assume that the damage affects the isochoric behaviour only, the free energy is additively split into an isochoric and a volumetric part $\Psi = \Psi_{\text{iso}} + \Psi_{\text{vol}}$ such that Eqs. (6) and (7) can be rewritten as

$$\mathbf{S} = \mathbf{S}_{\text{iso}} + \mathbf{S}_{\text{vol}} \quad \text{where} \quad \mathbf{S}_{\text{iso}} = 2 \frac{\partial \Psi_{\text{iso}}}{\partial \mathbf{C}}, \quad \mathbf{S}_{\text{vol}} = 2 \frac{\partial \Psi_{\text{vol}}}{\partial \mathbf{C}} \quad (8)$$

and

$$\mathcal{D}_m = -\frac{\partial \Psi_{\text{iso}}}{\partial \Gamma} \dot{\Gamma} = -\frac{\partial \Psi_{\text{iso}}}{\partial m} \frac{\partial m}{\partial \Gamma} \dot{\Gamma} = -\frac{\partial \Psi_{\text{iso}}}{\partial m} \dot{m} \geq 0 \quad (9)$$

with $\Psi_{\text{iso}} = \Psi_{\text{iso}}(\bar{\mathbf{C}}, m(\Gamma))$ and $\Psi_{\text{vol}} = \Psi_{\text{vol}}(J)$. Here, $m(\Gamma)$ can be replaced formally by $\eta(\Gamma)$, $d(\Gamma)$ or $X(\Gamma)$.

2.3 Parameter fitting

To find the best sets of parameters for the tested models in terms of the least mean squared error, a standard Trust-Region algorithm is used for the model calibration. The error is defined as the normalized deviation between the model and the experimental 1st Piola-Kirchhoff stress $\mathbf{P} = \mathbf{F} \cdot \mathbf{S}$ in loading direction x , viz. between $P_{xx,\text{mod}} = \lambda_x S_{xx,\text{mod}}$ and $P_{xx,\text{exp}}$. That leads to a minimisation problem with the following cost function

$$F(p_j) = \frac{1}{2} \left(\sum_{i=1}^{m_{\text{ux}}} \frac{r_i^2}{m_{\text{ux}}} + \sum_{i=1}^{m_{\text{ps}}} \frac{r_i^2}{m_{\text{ps}}} + \sum_{i=1}^{m_{\text{bx}}} \frac{r_i^2}{m_{\text{bx}}} \right) \rightarrow \min$$

with $r_i = \frac{P_{xx,\text{mod},i} - P_{xx,\text{exp},i}}{\max(P_{xx,\text{exp},i})}$

and $P_{xx,\text{mod},i} = \lambda_{x,i} S_{xx,\text{mod}}(\mathbf{F}_{\text{exp},i}, i-1, p_1, \dots, p_n)$ (10)

m_{ux} , m_{ps} , m_{bx} are the number of experimental observations, viz. the load increments, considered for fitting. $i-1$ and i refer to the beginning and the end, respectively, of the i -th increment. The abbreviations ux, ps and bx stand for the tested loading modes: uniaxial tension, pure shear and equibiaxial tension, cf. Sect. 4. The normalisation is carried out with respect to the maximum stress in the fitting range of each experiment. The division of the squared residuals r_i^2 by the number of experimental data points ensures an equal weight of all loading modes. n is the number of parameters. The model stress $S_{xx,\text{mod},i}$ is a function of the parameters p_j ($j = 1, \dots, n$), the history variable at the beginning of the current load step Γ_{i-1} (which must be updated to Γ_i) and the measured stretches. The stretches are turned into a corresponding deformation gradient $\mathbf{F}_{\text{exp},i}$ under the assumption of perfect incompressibility. This assumption is a good and pragmatic approximation for filled, technical elastomers up to moderate strains, see for example [26]. Due to the incompressibility, the volumetric stress contribution in Eq. (8) is not anymore computed from the volumetric free energy Ψ_{vol} as

$$\mathbf{S}_{\text{vol}} = 2 \frac{\partial \Psi_{\text{vol}}}{\partial \mathbf{C}} = -p \mathbf{J} \mathbf{C}^{-1} \quad \text{with} \quad p = -\frac{\partial \Psi_{\text{vol}}}{\partial J} \quad (11)$$

but is given by

$$\mathbf{S}_{\text{vol}} = -\bar{p} \mathbf{J} \mathbf{C}^{-1} \quad (12)$$

where the hydrostatic pressure \bar{p} stems from the stress-free condition in lateral direction.

To speed up the fitting procedure, an exact Jacobian is used within the least squares method. For material models with a history variable, it is obtained as

$$J_{ij} = \frac{dS_{xx,mod,i}}{dp_j} = \frac{\partial S_{xx,mod,i}}{\partial p_j} + \frac{\partial S_{xx,mod,i}}{\partial \Gamma_{i-1}} \frac{d\Gamma_{i-1}}{dp_j}. \quad (13)$$

Hence, at each time increment i , the history variable Γ_i as well as its derivatives with respect to the material parameters

$$\frac{d\Gamma_i}{dp_j} = \frac{\partial \Gamma_i}{\partial p_j} + \frac{\partial \Gamma_i}{\partial \Gamma_{i-1}} \frac{d\Gamma_{i-1}}{dp_j} \quad (14)$$

must be updated and stored.

As the Trust-Region algorithm is only locally convergent, the whole fitting procedure is repeated ten times with different, randomly generated initial guesses according to the Latin hypercube sampling. More precisely, for each parameter of a model, an initial guess range is prescribed which is equally divided into ten intervals. In each interval a random number is drawn from a uniform distribution. These values are then randomly combined to ten different sets of parameters which serve as the initial guesses for the fitting procedure.

2.4 Root mean squared error and correlation matrix

Since the normalized residual of the minimisation problem (10) is not very descriptive, the root mean squared error (RMSE) with respect to the absolute error

$$RMSE = \left(\frac{1}{m_{all}} \left(\sum_{i=1}^{m_{ux}} \bar{r}_i^2 + \sum_{i=1}^{m_{ps}} \bar{r}_i^2 + \sum_{i=1}^{m_{bx}} \bar{r}_i^2 \right) \right)^{\frac{1}{2}} \quad (15)$$

$$\text{where } \bar{r}_i = P_{xx,mod,i} - P_{xx,exp,i}$$

$$m_{all} = m_{ux} + m_{ps} + m_{bx}$$

is used for the discussion of the results. As explained in Sect. 5, not all experimental data points are considered for the fitting procedure. Instead, the data outside of the fitting range (i.e., inside the predicting range) is used to evaluate the predictivity of the models. For this purpose, Eq. (15) is applied analogously to the data in the predicting range yielding the root mean square prediction error (RMSPE).

One desirable property of material models is a low correlation between the parameters. The Pearson correlation matrix $[\rho_{ij}]$ is obtained from the covariance matrix $[D_{ij}]$ as

$$\rho_{ij} = \left| \frac{D_{ij}}{\sqrt{D_{ii} D_{jj}}} \right|. \quad (16)$$

In case of least square methods, the covariance matrix can be computed from the approximated Hessian $[H_{ij}]$, i.e., the 2nd derivative of the cost function $F(p_j)$ and the scaled mean square error

$$D_{ij} \approx \frac{(RMSE)^2}{m_{ux} + m_{ps} + m_{bx}} H_{ij}^{-1}, \quad (17)$$

see for example [14]. The correlation matrix component $\rho_{ij} \in [0, 1]$ describes the correlation between the i -th and j -th parameter. The matrix $[\rho_{ij}]$ is symmetric and $\rho_{ii} = 1 \forall i$. Values close to 0 represent a low correlation. Whereas values close to 1 indicate a high correlation stemming from either an overparameterised model or from an improper experiment which provides insufficient information about the material behaviour.

3 Damage models

3.1 Choice of basic hyperelastic models

As described in Sect. 1, the considered damage models must be combined with a basic hyperelastic model defined by its strain energy function Ψ_0 . To obtain a purely isochoric damage, Ψ_0 must be defined in terms of the isochoric right Cauchy-Green tensor $\bar{\mathbf{C}}$. Due to the endless list of proposed strain energy functions, we restrict ourselves to three promising models:

- (a) The polynomial approach with terms up to 6th order of deformation, i.e., up to $\bar{\lambda}^6$ where $\bar{I}_1 \propto \bar{\lambda}^2$ and $\bar{I}_2 \propto \bar{\lambda}^4$ [20] reads

$$\Psi_0 = c_{10} (\bar{I}_1 - 3) + c_{20} (\bar{I}_1 - 3)^2 + c_{30} (\bar{I}_1 - 3)^3 + c_{01} (\bar{I}_2 - 3) + c_{11} (\bar{I}_1 - 3) (\bar{I}_2 - 3) \quad (18)$$

with five parameters $c_{10}, c_{20}, c_{30}, c_{01}, c_{11} \in [0, \infty)$. The initial shear modulus is given by $G_0 = 2(c_{10} + c_{01})$. All material parameters units are shown in Table 6.

- (b) Alternatively, the invariants themselves can be exponentiated, see [40]. This approach leads to

$$\Psi_0 = \frac{3}{2} \left(\frac{A_1}{\alpha_1} \left(\left(\frac{\bar{I}_1}{3} \right)^{\alpha_1} - 1 \right) + \frac{A_2}{\alpha_2} \left(\left(\frac{\bar{I}_1}{3} \right)^{\alpha_2} - 1 \right) + \frac{B_1}{\beta_1} \left(\left(\frac{\bar{I}_2}{3} \right)^{\beta_1} - 1 \right) \right) \quad (19)$$

using six parameters $A_1, A_2, B_1 \in [0, \infty)$ and $\alpha_1, \alpha_2, \beta_1 \in (0, \infty)$. The initial shear modulus is obtained as $G_0 = A_1 + A_2 + B_1$. Similar to [40], the exponents are fixed to certain values rather than fitted because the Trust Region algorithm mostly tends to push them to very high or low values. This may lead to numerical problems and high parameter correlations. Here, the exponents are fixed according to the approach of [7]: $\alpha_1 = 1, \alpha_2 = 4, \beta_1 = \frac{1}{2}$.

- (c) A simplified version of the extended non-affine tube model from [21] was proposed by [35]:

$$\Psi_0 = \frac{G_c}{2} \frac{(\bar{I}_1 - 3)}{1 - \frac{1}{n} (\bar{I}_1 - 3)} + 3 G_e \left(\left(\frac{\bar{I}_2}{3} \right)^{\frac{1}{2}} - 1 \right) \quad (20)$$

with $G_c, G_e \in [0, \infty)$, $\frac{1}{n} \in [0, 1]$ and $G_0 = G_c + G_e$.

The criteria for the choice of these three models are as follows: The strain energy function must be formulated in a closed-form and in terms of elementary functions since some damage models use the basic strain energy as measure of maximum load. For this reason, the models by [1] as well as [25], among others, are not included here. The stress computation must not depend on numerical integration methods to minimize the computational effort. Therefore, the micro-sphere model by [30] is not considered here.

The following Sects. 3.2 to 3.4 explain in detail the three classes of damage models given in Sect. 2.2. In each of the sections, suitable model formulations from the literature are introduced which will be used for the comparison thereafter. To point out the different motivations of the model classes, Fig. 2 depicts qualitatively their behaviour.

3.2 Damage models with virgin state variable

The first group of damage models assumes that the basic strain energy function Ψ_0 describes the virgin state curve. For this purpose, a virgin state variable $\eta \in [0, 1]$ is introduced, such that

$$\mathbf{S}_{\text{iso}} = \eta \mathbf{S}_0 \quad \text{with} \quad \mathbf{S}_0 = 2 \frac{\partial \Psi_0}{\partial \mathbf{C}} \quad (21)$$

where $\eta = 1$ indicates a primary loading and $\eta \neq 1$ an un- or reloading. [33] coined the name pseudo-elasticity for this model type. The idea was first described by [11] and generalised by [32]. Furthermore, the latter authors proved that the only feasible choice for the scalar measure of maximum load is the basic strain

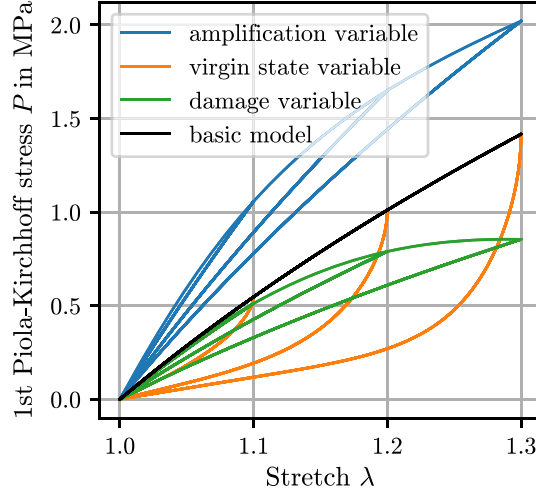


Fig. 2 Comparison of the three damage model classes: stress response to the input data from Fig. 1a of different damage models combined with the same basic hyperelastic model (for this illustration, a Neo-Hooke model is used which is obtained from strain energy function (b) with $\alpha_1 = 1$, $A_2 = 0$, $B_1 = 0$)

energy: $\Gamma = \Psi_{0,\max} = \max_{\bar{t} \in [0,t]}(\Psi_0(\bar{t}))$, i.e., the maximum value of the basic strain energy within the loading history. The total free energy reads

$$\Psi_{\text{iso}}(\Psi_0(\bar{C}), \Psi_{0,\max}) = \int_0^{\Psi_0} \eta(\bar{\Psi}_0, \Psi_{0,\max}) d\bar{\Psi}_0 \quad (22)$$

such that

$$\mathbf{S}_{\text{iso}} = 2 \frac{\partial \Psi_{\text{iso}}}{\partial \mathbf{C}} = 2 \frac{\partial \Psi_{\text{iso}}}{\partial \Psi_0} \frac{\partial \Psi_0}{\partial \mathbf{C}} = \eta \mathbf{S}_0 \quad (23)$$

and

$$\mathcal{D}_m = -\frac{\partial \Psi_{\text{iso}}}{\partial \Psi_{0,\max}} \dot{\Psi}_{0,\max} = -\dot{\Psi}_{0,\max} \int_0^{\Psi_0} \frac{\partial \eta}{\partial \Psi_{0,\max}} d\bar{\Psi}_0 \geq 0. \quad (24)$$

To define the function $\eta(\Psi_0, \Psi_{0,\max})$, two general approaches are presented in the literature. On the one hand, one can define $\eta = \eta\left(\frac{\Psi_0}{\Psi_{0,\max}}\right)$ with $\eta: [0, 1] \rightarrow [0, 1]$ and $\eta(1) = 1$. Here, the basic strain energy function must be restricted to $\Psi_0 \geq 0$ to ensure $\frac{\Psi_0}{\Psi_{0,\max}} \in [0, 1]$. Demanding η to be a monotonically increasing function $\frac{\partial \eta}{\partial \left(\frac{\Psi_0}{\Psi_{0,\max}}\right)} > 0$ is sufficient to fulfil inequality (24). This approach includes the model by [11]:

Model 1.1 [11] $\eta = a \tan\left(b \frac{\Psi_0}{\Psi_{0,\max}} - c\right) + d$

Unfortunately, the authors did not give an explicit formula for η but plots instead, see their Figs. 1 and 7. Thus, the function given above is a reconstructed approximation reproducing these plots. To ensure $\eta(1) = 1$ and to consider only the principal branch of the tangent, following three fitting parameters are defined: $c \in (0, \frac{\pi}{2})$, $\Delta b = b - c \in (0, \frac{\pi}{2})$ and $\eta_{\min} = \eta(\Psi_0 = 0) \in [0, 1)$ such that

$$\begin{aligned} a &= \frac{1 - \eta_{\min}}{\tan(\Delta b) + \tan(c)} \\ b &= c + \Delta b \\ d &= a \tan(c) + \eta_{\min}. \end{aligned} \quad (25)$$

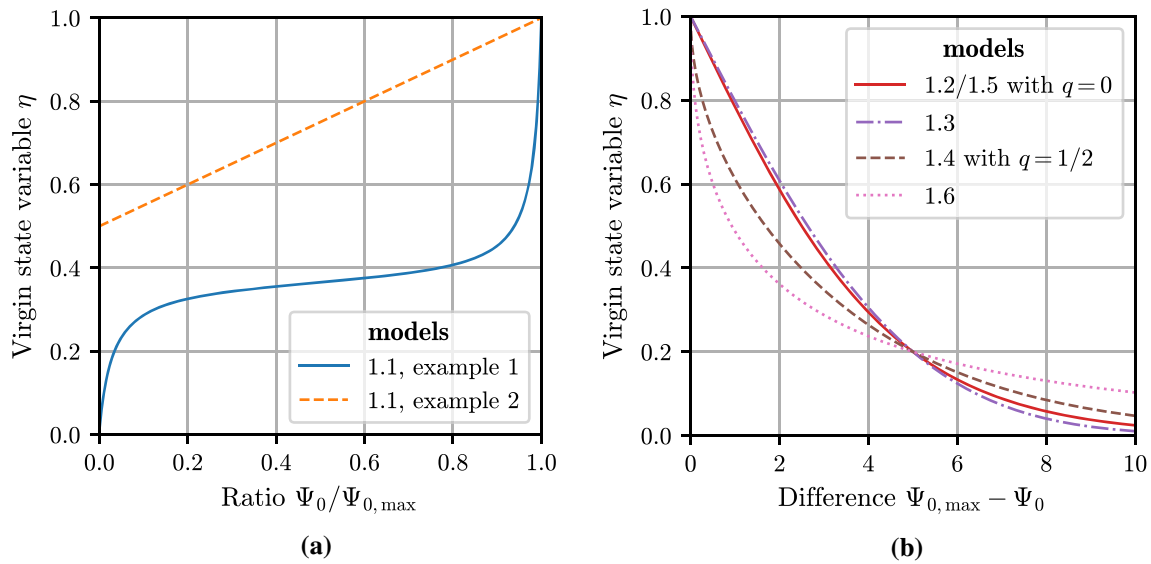


Fig. 3 Evolution of the virgin state variable η using **a** the approach $\eta(\Psi_0/\Psi_{0,\max})$ according to model 1.1 with two different parameter sets such that Figs. 1 and 7 from [11] are qualitatively reproduced and **b** the approach $\eta(\Psi_{0,\max} - \Psi_0)$ according to models 1.2 to 1.6 with $r = 1$ and m such that $\eta(5) = 0.2$

To prove the capability of the presented approximation, Fig. 3a depicts the reconstructed plots from [11].

The second general approach defines $\eta = \eta(\Psi_{0,\max} - \Psi_0)$ with $\eta : [0, \infty) \rightarrow [0, 1]$ and $\eta(0) = 1$. Then, $\frac{\partial \eta}{\partial (\Psi_{0,\max} - \Psi_0)} < 0$ is sufficient to fulfill inequality (24), see [32]. A discrepancy between these demands for monotonicity and experimental findings are discussed by [22]. Based on uniaxial tension tests with $\eta = \frac{(S_{xx} - S_{vol,xx})}{S_{0,xx}}$, they showed that η is in general non-monotonic. The second approach is applied for instance by

model 1.2 [13] $\eta = 1 - r \tanh(m (\Psi_{0,\max} - \Psi_0))$

model 1.3 [33] $\eta = 1 - r \operatorname{erf}(m (\Psi_{0,\max} - \Psi_0))$

model 1.4 [42] $\eta = 1 - r \tanh(m (\Psi_{0,\max} - \Psi_0))^q$

model 1.5 [5]

$$\eta = 1 - r \tanh\left(m \frac{(\Psi_{0,\max} - \Psi_0)}{(1+q)\Psi_{0,\max}}\right)$$

model 1.6 [15] $\eta = \exp\left(-\sqrt{m (\Psi_{0,\max} - \Psi_0)}\right)$

model 1.4* [42] modified²

$$\eta = 1 - r \sqrt{\tanh(m (\Psi_{0,\max} - \Psi_0))}$$

Model 1.6* [15] modified³

$$\eta = 1 - r \left(1 - \exp\left(-\sqrt{m (\Psi_{0,\max} - \Psi_0)}\right)\right)$$

The material parameters are $r \in [0, 1]$ and $m, q \in [0, \infty)$ and the units of all parameters are given in Table 6. The evolution equations are compared in Fig. 3b. Models that do not fulfil $\frac{\partial \eta}{\partial (\Psi_{0,\max} - \Psi_0)} < 0$ are not considered, for instance [41].

² The parameter $q = \frac{1}{2}$ is fixed to reduce the number of fitting parameters. Note that modified evolution equations will be indicated by an asterisk.

³ The parameter r is introduced in the present paper to improve the model capability.

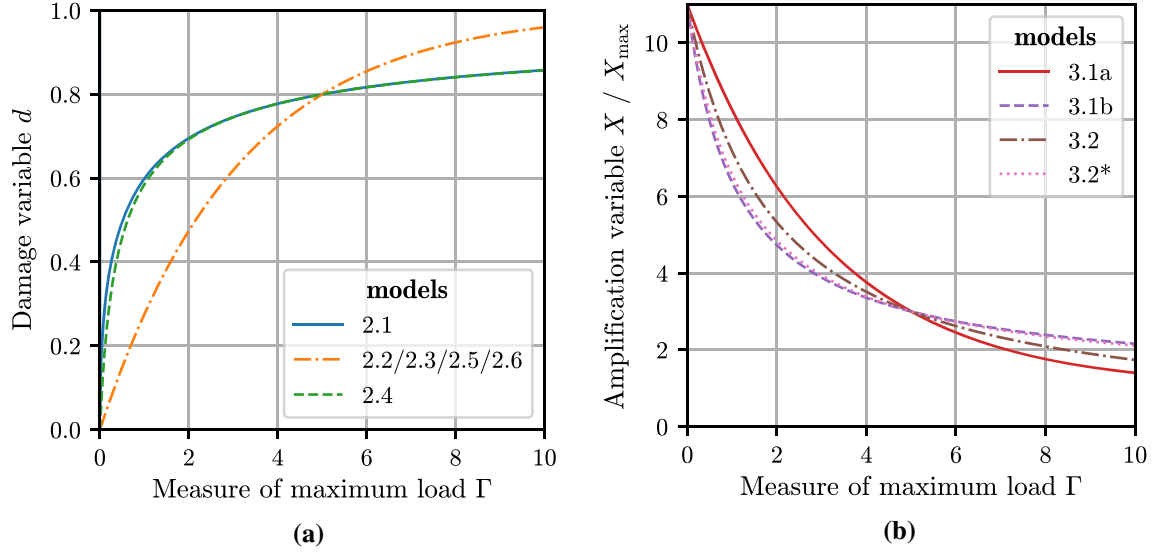


Fig. 4 Evolution of **a** the damage variable d according to models 2.1 to 2.6 with $\beta = 1$ and α such that $d(5) = 0.8$ and **b** the amplification variables X and X_{\max} according to models 3.1a/3.1b and 3.2/3.2* with $X_0 = 10$, $X_{\infty} = 1$, and γ such that $X(5) = 3$ and $X_{\max}(5) = 3$, respectively

3.3 Damage models with damage variable

The second class of damage models, as given in Sect. 2.2, introduces a damage variable which depends on the scalar measure of maximum load $d = d(\Gamma)$. The desired stress response is

$$\mathbf{S}_{\text{iso}} = (1 - d) \mathbf{S}_0 \quad \text{where} \quad \mathbf{S}_0 = 2 \frac{\partial \Psi_0}{\partial \mathbf{C}}. \quad (26)$$

Here, $d = 0$ denotes the virgin state and $d = 1$ a totally damaged material. The basic stress response \mathbf{S}_0 acts as an upper limit (if $d \rightarrow 0$). The corresponding damage evolution maps $d: [0, \infty) \rightarrow [0, 1]$ with $d(0) = 0$ and the free energy is given by

$$\Psi_{\text{iso}} = (1 - d) \Psi_0(\bar{\mathbf{C}}) \quad (27)$$

with the dissipation rate

$$\mathcal{D}_m = - \frac{\partial \Psi_{\text{iso}}}{\partial d} \dot{d} = \Psi_0 \frac{\partial d}{\partial \Gamma} \dot{\Gamma} \geq 0. \quad (28)$$

Since $\dot{\Gamma} \geq 0$, the restriction $\Psi_0 \frac{\partial d}{\partial \Gamma} \geq 0$ has to hold true for any deformation to fulfil inequality (28). This requirement cannot be satisfied without further restrictions on the basic strain energy because any constant term can be added to Ψ_0 without affecting the stress-deformation relation Eq. (9) but the extent and sign of dissipation. Thus, equal conditions are enforced by demanding $\Psi_0(\mathbf{I})$ to be a global minimum with $\Psi_0(\mathbf{I}) = 0$. The restriction reduces then to $\frac{\partial d}{\partial \Gamma} \geq 0$, i.e., d has to be a monotonically increasing function.

In contrast to the models using a virgin state variable, the measure of maximum load is not restricted to the basic strain energy and, hence, can be chosen more arbitrarily. The following list compiles the considered models along with the measure of maximum load and the damage evolution (cf. Fig 4a):

model 2.1 [38] $\Gamma = \Psi_{0,\max}$,

$$d(\Gamma) = \beta \left(1 - \frac{(1 - \exp(\sqrt{\alpha} \Gamma))}{(\sqrt{\alpha} \Gamma)} \right)$$

model 2.2 [29] $\Gamma = \Psi_{0,\max}$,

$$d(\Gamma) = \beta (1 - \exp(-\alpha \Gamma))$$

model 2.3 [8] $\Gamma = \sqrt{\frac{\bar{I}_{1,\max}}{3}} - 1,$
 $d(\Gamma) = \beta (1 - \exp(-\alpha \Gamma))$

model 2.4 [4]⁴ $\Gamma = \bar{C}_{\Gamma,\max}^2,$
 $d(\Gamma) = \beta \left(1 - \frac{1}{\sqrt{1+\alpha \Gamma}}\right)$

model 2.5 [2]⁵ $\Gamma = \frac{\|\bar{\mathbf{C}}\|_{\max}}{\sqrt{3}} - 1,$
 $d(\Gamma) = \beta (1 - \exp(-\alpha \Gamma))$

model 2.6 [24]⁶ $\Gamma = \bar{\lambda}_{\max} - 1,$
 $d(\Gamma) = \beta (1 - \exp(-\alpha \Gamma))$

model 2.4* [4] modified⁷ $\Gamma = \bar{C}_{\text{vM},\max}^2,$
 $d(\Gamma) = \beta \left(1 - \frac{1}{\sqrt{1+\alpha \Gamma}}\right)$

The material parameters are $\alpha \in [0, \infty)$ and $\beta \in [0, 1]$. See Table 6 for the parameter units.

3.4 Damage models with amplification variable

The previous two model classes are phenomenologically motivated. In contrast, the third class (cf. Sect. 2.2) is based on the physical concept of strain amplification. Due to the presence of rigid filler particles, an inhomogeneous deformation field and a locally amplified strain of the polymer chains is assumed. The introduction of an amplification variable X seems likely such that

$$(\bar{\lambda} - 1) = X (\bar{\lambda}_0 - 1) \quad (29)$$

with the macroscopic stretch $\bar{\lambda}_0$, see [31]. Moreover, a deformation of the rubber will lead to a breakdown of filler clusters and to a debonding of polymer chains from the filler particles, see for instance [12] for physical interpretations of the Mullins effect. The ruptured filler particles have a less amplifying effect on the polymer network, i.e., X decreases. Note that the considered approaches do not model the filler stress response itself, that is, the filler network has no load-bearing capacity (for a counterexample see [35] who added a filler contribution to the basic strain energy). Hence, the basic hyperelastic response $\mathbf{S}_0 = 2 \frac{\partial \psi_0}{\partial \mathbf{C}}$ can be interpreted as the response of an unfilled rubber which is equivalent to a totally damaged state containing broken filler clusters only. Thus, \mathbf{S}_0 is a lower limit for $X \rightarrow 1$.

From a numerical point of view, the strain amplification described above is unattractive since an eigenvalue computation is required for every model. Therefore, a more practicable amplification of the principle invariants is introduced. In contrast to [3] who presented an invariant amplification restricted to the Neo-Hooke model, a more general approach suitable for many invariant-based strain energy functions is proposed here. Noting that $\bar{I}_1 \propto \bar{\lambda}^2$ and $\bar{I}_2 \propto \bar{\lambda}^4$, a feasible, consistent amplification is given by following replacements

$$\begin{aligned} (\bar{I}_1 - 3)^k &\rightarrow X^k (\bar{I}_1 - 3)^k \\ (\bar{I}_2 - 3)^k &\rightarrow X^{2k} (\bar{I}_2 - 3)^k \end{aligned} \quad (30)$$

⁴ $\bar{C}_{\Gamma} = \max(\bar{\lambda}_x^2 - \bar{\lambda}_y^2, \bar{\lambda}_y^2 - \bar{\lambda}_z^2, \bar{\lambda}_z^2 - \bar{\lambda}_x^2)$ denotes the Tresca invariant of the isochoric right Cauchy-Green tensor.

⁵ $\|\cdot\|$ denotes the Frobenius norm.

⁶ $\bar{\lambda}_{\max}$ denotes the maximum isochoric stretch.

⁷ $\bar{C}_{\text{vM}} = \sqrt{-3 I_2(\bar{\mathbf{C}}^{\text{D}})}$ with $\bar{\mathbf{C}}^{\text{D}} = \bar{\mathbf{C}} - \frac{\text{tr}(\bar{\mathbf{C}})}{3} \mathbf{I}$ denotes the von Mises invariant of the isochoric right Cauchy-Green tensor. In contrast to the Tresca invariant of the original model 2.4, the computation of eigenvalues is avoided.

and

$$\begin{aligned} \left(\left(\frac{\bar{I}_1}{3} \right)^k - 1 \right) &\rightarrow X^k \left(\left(\frac{\bar{I}_1}{3} \right)^k - 1 \right) \\ \left(\left(\frac{\bar{I}_2}{3} \right)^k - 1 \right) &\rightarrow X^{2k} \left(\left(\frac{\bar{I}_2}{3} \right)^k - 1 \right). \end{aligned} \quad (31)$$

The former replacement Eq. (30) is applicable to the basic strain energy function (a) from Sect. 3.1, whereas the latter replacement Eq. (31) is suitable for strain energy function (b). In case of (c), Eq. (30) is used for the \bar{I}_1 -part and Eq. (31) for the \bar{I}_2 -part. Amplified strain energy functions that are obtained by applying the replacements Eq. (30) or (31) to a basic strain energy functions Ψ_0 will be denoted by $\Psi_0^*(X, \bar{I}_1, \bar{I}_2)$.

Since the limitations pointed out in Sect. 1 lead to narrow confines of the paper's scope, a lot of highly specialised approaches are not considered here. Thus, besides the amplification concept, no further physically or micro-mechanically motivated models are discussed. For an overview of such sophisticated models, the reader is referred to [12].

The principle of strain amplification was considered for instance by [23]. Originally, they applied the strain amplification according to Eq. (29) to a generalized tube model. However, the more convenient invariant amplification (cf. Eqs. (30) and (31)) is used here such that

$$\Psi_{\text{iso}} = \Psi_0^*. \quad (32)$$

[23] proposed two evolution equations reading

$$\begin{aligned} \text{model 3.1a} \quad [34] \quad &\Gamma = \bar{\lambda}_{\text{max}} - 1, \\ &X(\Gamma) = (X_0 - X_\infty) \exp(-\gamma \Gamma) + X_\infty \\ \text{model 3.1b} \quad [34] \quad &\Gamma = \bar{\lambda}_{\text{max}} - 1, \\ &X(\Gamma) = (X_0 - X_\infty) (\Gamma + 1)^{-\gamma} + X_\infty \end{aligned}$$

with the material parameters $\Delta X_0 = (X_0 - X_\infty) \in [0, \infty)$, $X_\infty \in [1, \infty)$ and $\gamma \in [0, \infty)$. Noting that $\dot{X} = \frac{\partial X}{\partial \Gamma} \dot{\Gamma} \leq 0$ and $\dot{\Gamma} \geq 0$, the inequality

$$\mathcal{D}_m = -\frac{\partial \Psi_{\text{iso}}}{\partial X} \frac{\partial X}{\partial \Gamma} \dot{\Gamma} \geq 0 \quad (33)$$

can be satisfied by $\frac{\partial \Psi_{\text{iso}}}{\partial X} \geq 0$ and $\frac{\partial X}{\partial \Gamma} \leq 0$. The former inequality is fulfilled if Ψ_0 is a monotonic function w.r.t. the principal invariants and an amplification according to Eq. (30) or Eq. (31) is assumed. Whereas the latter inequality demands a monotonically decreasing evolution equation $X(\Gamma)$.

Another generalisable model is outlined by [34]. They assumed a non-uniform distribution of strain amplifying filler domains on the micro-mechanical scale and presented a mathematical homogenisation to obtain a representative, macroscopic free energy function. Transferring their approach to arbitrary strain energy functions in terms of principal invariants, one obtains

$$\Psi_{\text{iso}}(X_{\text{max}}, \bar{I}_1, \bar{I}_2) = \int_1^{X_{\text{max}}} P(X, X_{\text{max}}) \Psi_0^*(X, \bar{I}_1, \bar{I}_2) dX \quad (34)$$

where P denotes the distribution of the local amplification X which can be represented as

$$\begin{aligned} P(X, X_{\text{max}}) &= p(X) n(X_{\text{max}}) \quad \text{with} \\ p(X) &> 0 \quad \forall X \quad \text{and} \quad n(X_{\text{max}}) = \left(\int_1^{X_{\text{max}}} p(X) dX \right)^{-1}. \end{aligned} \quad (35)$$

The integration limits 1 and X_{max} represent the range from non-amplified to the maximum amplified domains. [34] suggested a power law distribution

$$p(X) = X^{-\chi} \quad \Rightarrow \quad n(X_{\text{max}}) = \frac{\chi - 1}{1 - X_{\text{max}}^{1-\chi}}. \quad (36)$$

Their evolution equation and the measure of maximum load read

model 3.2 [34] $\Gamma = \bar{I}_{1,\max} - 3$,

$$X_{\max}(\Gamma) = \max\left(X_{\max,\infty}, \frac{X_{\max,0}}{(\gamma\Gamma+1)}\right)$$

model 3.2* [34] modified⁸ $\Gamma = \bar{I}_{1,\max} - 3$,

$$X_{\max}(\Gamma) = \frac{(X_{\max,0} - X_{\max,\infty})}{(\gamma\Gamma+1)} + X_{\max,\infty}$$

Note that the parameters $X_{\max,0} = X_{\max}(0) = 1000$ and $X_{\max,\infty} = X_{\max}(\Gamma \rightarrow \infty) = 1$ are fixed to minimize the number of fitting parameters and their correlation. The remaining parameters are $\chi \in [1, \infty)$ and $\gamma \in [0, \infty)$.

The mechanical dissipation rate is obtained by

$$\mathcal{D}_m = -\frac{\partial \Psi_{\text{iso}}}{\partial X_{\max}} \frac{\partial X_{\max}}{\partial t} \geq 0. \quad (37)$$

Since $-\frac{\partial X_{\max}}{\partial \Gamma} \geq 0$ and $\dot{\Gamma} \geq 0$ by construction, $\frac{\partial \Psi_{\text{iso}}}{\partial X_{\max}} \geq 0$ has to be proven:

$$\frac{\partial \Psi_{\text{iso}}}{\partial X_{\max}} = \frac{\partial n(X_{\max})}{\partial X_{\max}} \int_1^{X_{\max}} p(X) \Psi_0^*(X, \bar{I}_1, \bar{I}_2) dX + n(X_{\max}) p(X_{\max}) \Psi_0^*(X_{\max}, \bar{I}_1, \bar{I}_2) \geq 0. \quad (38)$$

Using Eq. (35)₃, this is equivalent to

$$\Psi_0^*(X_{\max}, \bar{I}_1, \bar{I}_2) \int_1^{X_{\max}} p(X) dX \geq \int_1^{X_{\max}} p(X) \Psi_0^*(X, \bar{I}_1, \bar{I}_2) dX. \quad (39)$$

The first mean value theorem states, $\exists k \in [1, X_{\max}]$ such that

$$\int_1^{X_{\max}} p(X) \Psi_0^*(X, \bar{I}_1, \bar{I}_2) dX = \Psi_0^*(k, \bar{I}_1, \bar{I}_2) \int_1^{X_{\max}} p(X) dX \quad (40)$$

and, hence,

$$\Psi_0^*(X_{\max}, \bar{I}_1, \bar{I}_2) \int_1^{X_{\max}} p(X) dX \geq \Psi_0^*(k, \bar{I}_1, \bar{I}_2) \int_1^{X_{\max}} p(X) dX. \quad (41)$$

Note that, if $\frac{\partial \Psi_0^*(X, \bar{I}_1, \bar{I}_2)}{\partial X} \geq 0$, then $\Psi_0^*(X_{\max}, \bar{I}_1, \bar{I}_2) \geq \Psi_0^*(k, \bar{I}_1, \bar{I}_2) \forall k \in [1, X_{\max}]$ holds true and Eq. (41) is fulfilled for any k . Thus, similar to the approach by [23], an amplification according to Eq. (30) or Eq. (31) along with a monotonically increasing function Ψ_0^* w.r.t. the principal invariants are sufficient conditions for thermodynamic consistency.

4 Experiments

For illustration of the applicability of damage models, two filled elastomers possessing different mechanical behaviour are experimentally tested: a highly silica filled, sulphur-linked solution-styrene butadiene rubber (S-SBR, referred to as stiff compound, see Fig. 5a) and a lowly carbon black filled, sulphur-linked polybutadien/polyisoprene blend which tends to strain-induced crystallisation (BR/IR, referred to as soft compound, see Fig. 5b). Herein and in the following, quantities without indices refer to the loading direction.

For each material, quasi-static ($\dot{\lambda} = 0.01 \frac{1}{s}$) multihysteresis experiments were conducted under uniaxial, planar (pure shear) and equibiaxial tension. For this purpose, the material was loaded in a cyclic manner with

⁸ This modification provides a continuously differentiable evolution equation.

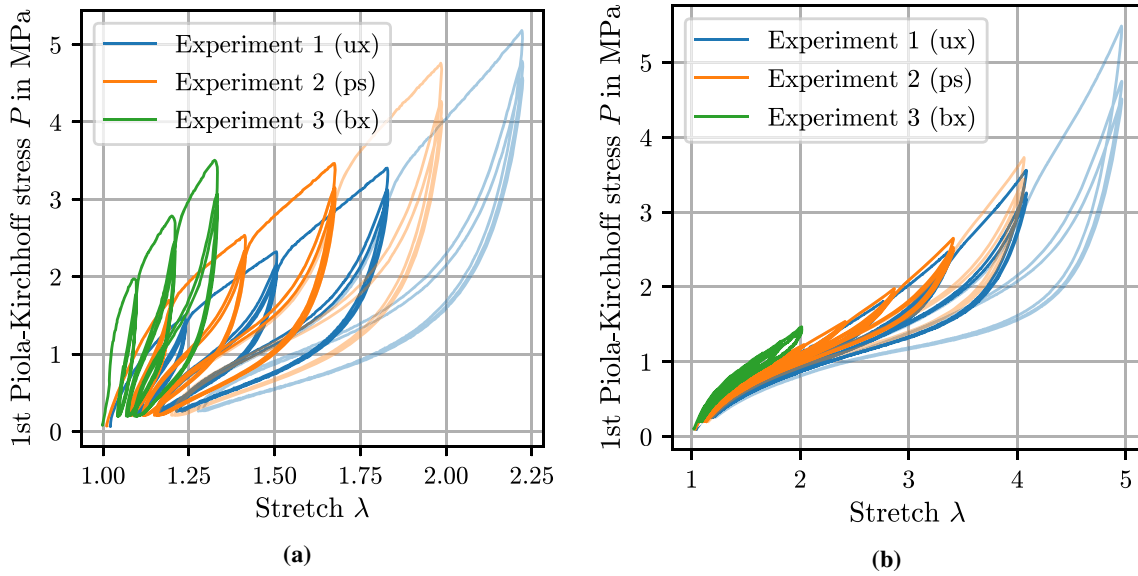


Fig. 5 Experimental data of the **a** stiff compound and **b** soft compound (the transparent cycles are not considered for fitting but employed to investigate the predictivity of the models)

Table 1 Strain amplitudes (engineering strain in %) of the multihysteresis experiments

No.	Uniaxial	Planar	Equibiaxial
1	21.48	18.36	10.22
2	47.58	40.13	21.48
3	79.28	65.99	33.90
4	117.79	96.76	47.58
5	164.58	133.47	62.66
6	221.41	177.35	79.28
7	290.45	229.89	97.60
8	374.33	292.94	117.79
9	476.22	368.71	140.05
10	600.00	459.93	164.58

three cycles per amplitude. Here, the amplitude levels for the uniaxial case were spaced logarithmically in the stretch domain because the extend of softening increases approximately logarithmically. The amplitudes are given in Table 1. To find equivalent strain amplitudes for the planar and equibiaxial deformation which generate a similar extend of softening, the concept of the invariant radius \bar{I}_r is introduced. For this purpose, the principle invariants are plotted in a parametric representation for each loading mode, see Fig. 6. Then, circles with the center (3, 3) are drawn in the invariant plane. The circle's radii are defined by the uniaxial amplitude levels, viz. $\bar{I}_r^2 = (\bar{I}_{1,ux} - 3)^2 + (\bar{I}_{2,ux} - 3)^2$. The intersection with the planar and equibiaxial curves provide the corresponding amplitudes of these deformation modes. The obtained data of the multihysteresis experiments are used for the parameter fitting whose results are discussed in the following section.

5 Results and discussion

5.1 Stiff compound

For the stiff compound, the first three amplitude levels of all three deformation modes were considered for fitting. The fourth amplitude levels of the uniaxial and planar tension test were used to prove the predictivity of the models. Fig. 7a and Table 2 show the ranking of all damage models sorted by the cost function value (10). Only the best combinations regarding the hyperelastic model are considered for the ranking.

Studying the effect of the basic model in Fig. 7a, two general things can be stated: The choice of the basic hyperelastic model is related to the model class of the damage model, e.g., all models using a damage

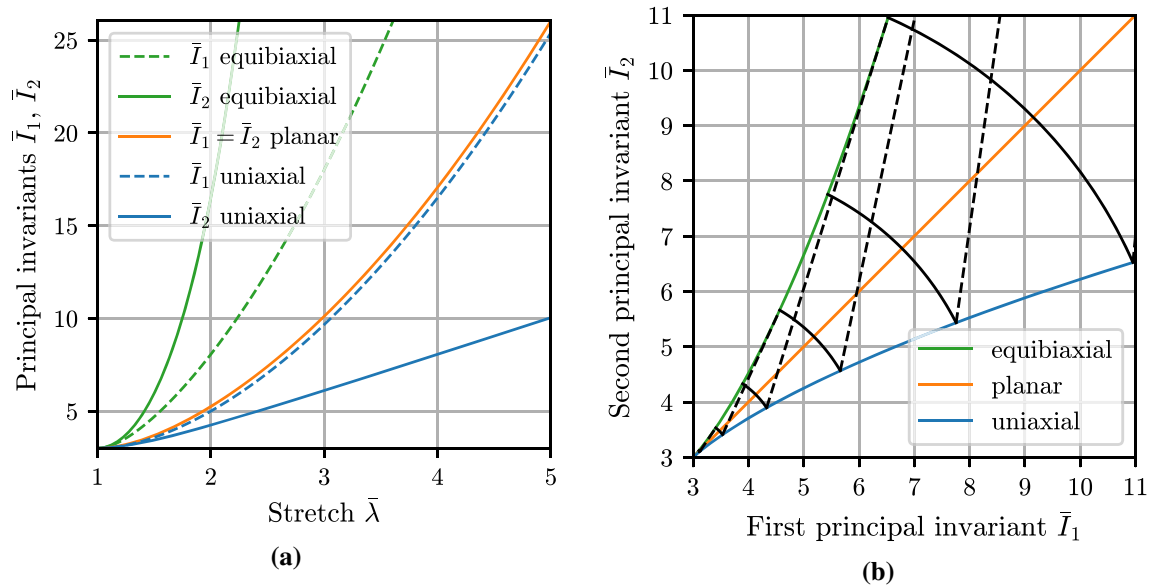


Fig. 6 **a** Principal invariants as a function of the stretch for the uniaxial, planar and equibiaxial tension test and **b** the corresponding parametric representations with iso-stretch curves (dashed, black lines) and invariant radii (solid, black lines)

Table 2 Ranking of the damage models regarding the stiff compound sorted by the cost function value, cf. Eq. (10)

Mod. No.	Reference	Basic Mod.	Parameters	Cost function	RMSE	RMSPE	Mean correlation	Mod. Calls
1.6*	[15] modified	(b)	2+3	0.1204	0.4180	0.5911	0.3963	18
3.2	[34]	(c)	2+3	0.1205	0.4185	0.4449	0.8034	67
1.4	[42]	(b)	3+3	0.1205	0.4186	0.5757	0.3435	18
1.6	[15]	(b)	1+3	0.1206	0.4188	0.6337	0.4586	16
1.4*	[42] modified	(b)	2+3	0.1222	0.4245	0.5684	0.3968	20
3.2*	[34] modified	(c)	2+3	0.1235	0.4291	0.6571	0.6232	60
1.1	[11]	(b)	3+3	0.1242	0.4316	0.4930	0.3716	20
1.5	[5]	(b)	3+3	0.1268	0.4407	0.4983	0.3710	23
1.2	[13]	(c)	2+3	0.1316	0.4570	0.5881	0.3801	20
1.3	[33]	(c)	2+3	0.1332	0.4627	0.5891	0.3752	22
2.3	[8]	(a)	2+5	0.1427	0.4949	2.0293	0.3810	25
2.1	[38]	(a)	2+5	0.1460	0.5064	0.6444	0.4112	32
2.5	[2]	(a)	2+5	0.1497	0.5191	2.6650	0.4099	22
2.2	[29]	(a)	2+5	0.1519	0.5268	2.9646	0.4323	40
2.4	[4]	(a)	2+5	0.1696	0.5889	0.6908	0.3626	43
2.4*	[4] modified	(a)	2+5	0.1696	0.5889	0.6908	0.3627	72
3.1b	[23]	(a)	3+5	0.1911	0.6620	1.3833	0.5436	25
2.6	[24]	(a)	2+5	0.1914	0.6646	1.5092	0.3957	38
3.1a	[23]	(b)	3+3	0.1927	0.6691	1.3027	0.5624	44

variable provide the best results if combined with the hyperelastic approach (a) by [20]. Generally, the basic hyperelastic model (a) is a reasonable overall choice for the stiff compound. However, the virgin state variable models are less sensitive to the employed basic model and tend slightly to prefer strain energy function (b). The models 3.1a/b are insensitive to the basic model, too, whereas the combination of models 3.2/3.2* with strain energy function (b) should be avoided. A second conclusion is that those models with a virgin state variable and models 3.2/3.2* are clearly the better choice for this material. However, note that the approach 2.4 by [4] is just one part of a more sophisticated model and, for sure, yields better results taking the full model into account.

Notably is also the difference between the performance of the damage models with an amplification variable. Apparently, the simpler amplification approach 3.1a/b is not sufficient to reproduce the complex softening behaviour of the tested materials. In contrast, model 3.2 provides a good trade-off between fitting quality and number of parameters. Though, the high number of model calls needed to find optimal parameter set and their quite high correlations are a slight drawback. The reader should keep in mind that the models 3.1a/b

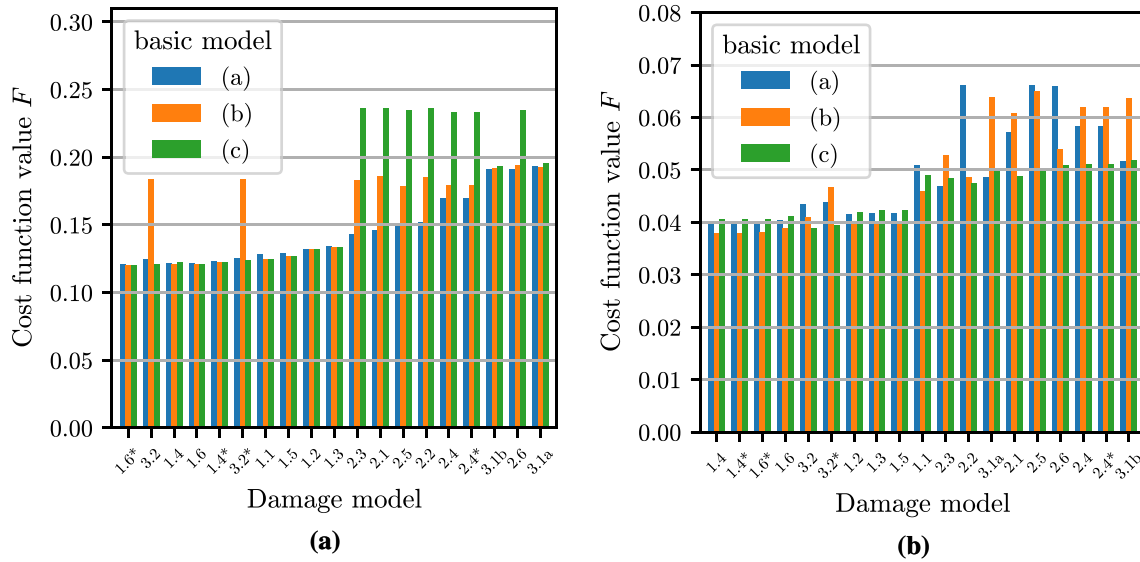


Fig. 7 Cost function values of all models with optimised parameters for **a** the stiff compound and **b** the soft compound

and 3.2 are tailor-made for tube models and needed slight modifications to make them generalisable to other hyperelastic models, see Sect. 3.4.

Remarkably, the RMSPE of all models do not show a clear trend, cf. Table 2. In case of models using a virgin state variable, it can be explained by the provided data. For these models, the basic strain energy describes the virgin curve, see Fig. 2. Since the virgin curve of the stiff compound does not include an upturn, see Fig. 5a, all parameters related to the upturn are indeterminate to some extent.

We like to point out another property of the virgin state variable models which does not appear in the ranking. In contrast to the remaining approaches, these models provide a pretty small correlation between the parameters stemming from the basic strain energy and from the damage model itself, see also Fig. 8d. That is, there is no undesired coupling which may lead to physically unlikely or unforeseen behaviour. Moreover, the η -functions of the best ranked virgin-state variable models 1.6 and 1.4 (as well as their modifications) are defined via a square root and an exponent $q < 1$, respectively, leading to an infinite slope for $\Psi_0 \rightarrow \Psi_{0,\max}$, cf. Fig. 3b. This behaviour seems to be essential for good fitting results since it represents the steep stress decrease after the turning point between a virgin loading and an unloading. Though, a slight drawback is to be expected considering a finite element implementation that requires a material tangent, i.e., the second derivative of the free energy with respect to the deformation. Since the derivative of η is indeterminate due to the infinite slope, a special numerical treatment is needed.

The proposed modifications indicated by an asterisk seem to be reasonable. The extended model 1.6* with only two parameters ranked first. The reduced model 1.4* lowers the parameter correlations and the RMSPE compared to model 1.4 without affecting the cost function value significantly. Also the result of model 3.2* with a continuously differentiable evolution equation is negligibly different to the original formulation. Model 2.4* avoids the computation of eigenvalues by replacing the Tresca invariant of model 2.4 by the von Mises invariant which has no impact on the fitting result. These conclusions for the presented modifications are affirmed by the results of the second compound, see Fig. 7b.

All fitted parameters are given in Table 4. The results of the best ranked model 1.6* are depicted in Fig. 8. One should keep in mind that each amplitude was cycled three times. Therefore, a much higher weight is given to un- and reloading curves in comparison with the virgin load.

5.2 Soft compound

Seven amplitude levels of each of the equibiaxial, planar, and uniaxial tests were considered for the fitting with the soft compound. The data of the eighth amplitude of the uniaxial and planar tension test provide an insight into the predictivity. Comparing the ranking regarding the soft compound in Fig. 7b and Table 3 with the results from the stiff compound, the much smaller RMSE of all models is conspicuous. This is related to

Table 3 Ranking of the damage models regarding the soft compound sorted by the cost function value, cf. Eq. (10)

Mod. No.	Reference	Basic Mod.	Parameters	Cost Function	RMSE	RMSPE	Mean Correlation	Mod. Calls
1.4	[42]	(b)	3+3	0.0379	0.0964	0.4382	0.3989	108
1.4*	[42]	(b)	2+3	0.0380	0.0965	0.4413	0.4506	27
1.6*	[15] modified	(b)	2+3	0.0381	0.0974	0.4260	0.4229	33
1.6	[15]	(b)	1+3	0.0388	0.1010	0.3950	0.5623	20
3.2	[34]	(c)	2+3	0.0389	0.0988	0.3081	0.6043	38
3.2*	[34] modified	(c)	2+3	0.0394	0.1026	0.3361	0.7258	38
1.2	[13]	(b)	2+3	0.0396	0.1010	0.4741	0.4448	28
1.3	[33]	(b)	2+3	0.0398	0.1016	0.4766	0.4462	31
1.5	[5]	(b)	3+3	0.0398	0.1016	0.4766	0.3987	34
1.1	[11]	(b)	3+3	0.0460	0.1233	0.5032	0.3609	43
2.3	[8]	(a)	2+5	0.0468	0.1287	0.5013	0.4818	104
2.2	[29]	(c)	2+3	0.0474	0.1317	0.3954	0.3501	67
3.1a	[23]	(a)	3+5	0.0486	0.1316	0.4578	0.5520	382
2.1	[38]	(c)	2+3	0.0487	0.1360	0.4740	0.4163	115
2.5	[2]	(c)	2+3	0.0501	0.1371	0.5648	0.3664	17
2.6	[24]	(c)	2+3	0.0508	0.1412	0.4876	0.4030	90
2.4	[4]	(c)	2+3	0.0510	0.1385	0.4866	0.3800	116
2.4*	[4] modified	(c)	2+3	0.0510	0.1385	0.4866	0.3800	129
3.1b	[23]	(a)	3+5	0.0517	0.1454	0.5665	0.5826	77

the fact, that the soft material is dominated by strain-induced crystallization rather than the Mullins effect. As a consequence, the permanent set which cannot be reproduced by the idealized damage models, cf. Fig. 1, is less pronounced, cf. Fig. 5b. Hence, better fits will be obtained for this material.

Like for the stiff compound, the virgin state variable models 1.4/1.4* [42] and 1.6/1.6* [15] combined with the strain energy function (b) by [40] achieved top rankings. They also show a quite low RMSPE indicating a good predictivity. The other virgin state variable models, except model 1.1, provide sound fitting quality, too.

In contrast to the stiff compound, strain energy function (c) is a good overall choice of the basic hyperelastic model. However, the virgin state variable models are again largely insensitive to the basic model and tend to better results if combined with strain energy function (b).

The model 3.2 by [34] in combination with basic model (c) shows also remarkable performance and is placed closely behind model 1.6. The results are depicted in Fig. 9. It is a promising alternative to the models with a virgin state variable. Note that in general models 3.2/3.2* should be preferably combined with strain energy function (c), cf. Fig. 7.

Models with a damage variable are less satisfactory again. However, in contrast to the stiff compound results, they are not far behind the models with a virgin state variable and may also be combined with basic model (c). Comparing models 2.2, 2.3, 2.5, 2.6 which use the same exponential evolution equation but different measures of maximum load, the approach 2.3 by [8] with $\Gamma = \sqrt{\frac{\bar{I}_{1,\max}}{3}} - 1$ seems to be the better choice. Further, the comparison between model 2.1 and 2.2 which both define $\Gamma = \Psi_{0,\max}$ but employ different evolution equations indicates that an exponential evolution as used by model 2.2 is probably not the best choice.

6 Conclusion

Fifteen common approaches to model the characteristic Mullins-effect of rubber materials in a discontinuous way were analysed. After discussing the possible range of applications, these models were classified by the type of their internal variable, proven to be thermodynamically consistent, and reasonable modification are proposed. Then, their ability for reproducing multihysteresis experiments of two different filled rubber compounds, referred to as stiff and soft compound, were tested. For this purpose, each damage model was combined with three different basic hyperelastic models and fitted to the experimental data. Thus, $19 \times 3 \times 2 = 114$ fittings were conducted. Rankings for both the soft and stiff compound sorted by the fitting quality were compiled. Moreover, the root mean square prediction error (RMSPE), parameter correlations, number of parameters as well as the number of model calls needed for the fitting procedure were discussed.

For the presented materials, the damage models with a virgin state variable in combination with the hyperelastic function by [40] referred to as basic model (b) seem to be a good overall choice. In particular, the

models by [15] and [42] (as well as their modifications) ranked in the top five for both materials. An alternative to the models with a virgin state variable is the approach by [34] based on the concept of strain amplification. Its combination with the simplified tube model by [35] referred to as basic model (c) provides sound fitting results. Models based on a damage variable lead to less satisfactory fits. In summary, even if several aspects of the complex mechanical material behaviour of elastomers are neglected, the considered damage models offer quick insights and a reasonable predictability for certain applications at low numerical costs. Moreover, the presented investigations may be used as a starting point for improving more complex models for rubber materials.

Acknowledgements We would like to thank Bayrak Lastik Sanayi ve Ticaret A.Ş., Freudenberg SE, Goodyear Innovation Center Luxembourg and Schüco International KG for financial support, and in particular, Goodyear for providing the materials. Moreover, we greatly appreciated the fruitful discussion with Jan Plagge, University of Wuppertal, and Meike Gierig, Leibniz University Hannover.

Funding Open Access funding enabled and organized by Projekt DEAL.

Open Access This article is licensed under a Creative Commons Attribution 4.0 International License, which permits use, sharing, adaptation, distribution and reproduction in any medium or format, as long as you give appropriate credit to the original author(s) and the source, provide a link to the Creative Commons licence, and indicate if changes were made. The images or other third party material in this article are included in the article's Creative Commons licence, unless indicated otherwise in a credit line to the material. If material is not included in the article's Creative Commons licence and your intended use is not permitted by statutory regulation or exceeds the permitted use, you will need to obtain permission directly from the copyright holder. To view a copy of this licence, visit <http://creativecommons.org/licenses/by/4.0/>.

Declarations

Conflict of interest The authors declare that they have no conflict of interest.

Appendix:A Fitted parameters

Table 4 Fitted parameters of the damage models for the stiff compound (see Table 6 for the parameter units)

Mod. No.	Damage Parameters			Basic Mod.	Hyperelastic Parameters				
1.1	$c =$ 1.2484	$\Delta b =$ 1.3258	$\eta_{\min} =$ 0.0	(b)	$A_1 =$ 1.5388	$A_2 =$ 0.0	$B_1 =$ 1.0743		
1.2	$m =$ 3.5432	$r =$ 0.6223		(c)	$G_c =$ 1.4377	$G_e =$ 0.9469	$1/n =$ 0.0446		
1.3	$m =$ 3.0020	$r =$ 0.6132		(c)	$G_c =$ 1.4197	$G_e =$ 0.9813	$1/n =$ 0.0585		
1.4	$m =$ 0.8571	$r =$ 0.7750	$q =$ 0.3570	(b)	$A_1 =$ 1.4277	$A_2 =$ 0.0772	$B_1 =$ 1.0883		
1.4*	$m =$ 1.6622	$r =$ 0.6948		(b)	$A_1 =$ 1.4499	$A_2 =$ 0.0647	$B_1 =$ 1.0188		
1.5	$m =$ 7.7733	$r =$ 0.6431	$q =$ 1.8281	(b)	$A_1 =$ 1.5235	$A_2 =$ 0.0	$B_1 =$ 0.9538		
1.6	$m =$ 1.3336			(b)	$A_1 =$ 1.4555	$A_2 =$ 0.0599	$B_1 =$ 1.0570		
1.6*	$m =$ 1.8599	$r =$ 0.9078		(b)	$A_1 =$ 1.4412	$A_2 =$ 0.0720	$B_1 =$ 1.0672		
2.1	$\alpha =$ 7.1114	$\beta =$ 0.9999		(a)	$c_{10} =$ 0.0	$c_{20} =$ 5.4091	$c_{30} =$ 0.04.38	$c_{01} =$ 3.9729	$c_{11} =$ 7.5252
2.2	$\alpha =$ 1.2961	$\beta =$ 0.8322		(a)	$c_{10} =$ 0.0	$c_{20} =$ 0.0	$c_{30} =$ 0.4367	$c_{01} =$ 0.9630	$c_{11} =$ 1.2714
2.3	$\alpha =$ 19.2526	$\beta =$ 0.9368		(a)	$c_{10} =$ 0.4187	$c_{20} =$ 1.4479	$c_{30} =$ 0.8491	$c_{01} =$ 0.6718	$c_{11} =$ 1.1938
2.4	$\alpha =$ 72.0576	$\beta =$ 0.9999		(a)	$c_{10} =$ 3.9482	$c_{20} =$ 5.7364	$c_{30} =$ 0.0	$c_{01} =$ 0.5334	$c_{11} =$ 0.0768
2.4*	$\alpha =$ 71.6160	$\beta =$ 0.9999		(a)	$c_{10} =$ 3.9369	$c_{20} =$ 5.7184	$c_{30} =$ 0.0	$c_{01} =$ 0.5317	$c_{11} =$ 0.0764
2.5	$\alpha =$ 1.0468	$\beta =$ 0.9589		(a)	$c_{10} =$ 1.9690	$c_{20} =$ 3.8691	$c_{30} =$ 1.4843	$c_{01} =$ 0.1506	$c_{11} =$ 0.2763
2.6*	$\alpha =$ 3.9236	$\beta =$ 0.8843		(a)	$c_{10} =$ 1.4738	$c_{20} =$ 1.0424	$c_{30} =$ 0.2772	$c_{01} =$ 0.0	$c_{11} =$ 0.0
3.1a	$\Delta X_0 =$ 1.7946	$X_\infty =$ 2.4279	$\gamma =$ 2.4162	(b)	$A_1 =$ 0.0	$A_2 =$ 0.0108	$B_1 =$ 0.0		
3.1b	$\Delta X_0 =$ 7.7384	$X_\infty =$ 1.3980	$\gamma =$ 7.4574	(a)	$c_{10} =$ 0.1789	$c_{20} =$ 0.0947	$c_{30} =$ 0.00171	$c_{01} =$ 0.0	$c_{11} =$ 0.0
3.2	$\chi =$ 1.8395	$\gamma =$ 11.6253		(a)	$G_c =$ 0.1549	$G_e =$ 0.1317	$1/n =$ 0.099		
3.2*	$\chi =$ 1.6776	$\gamma =$ 50.5140		(a)	$G_c =$ 0.1024	$G_e =$ 0.0776	$1/n =$ 0.0422		

Table 5 Fitted parameters of the damage models for the soft compound (see Table 6 for the parameter units)

Mod. No.	damage parameters			Basic Mod.	hyperelastic parameters					
1.1	$c =$ 0.0	$\Delta b =$ 1.3983	$\eta_{\min} =$ 0.8035	(b)	$A_1 =$ 0.6198	$A_2 =$ = 0.00077	$B_1 =$ 0.0697			
1.2	$m =$ 1.0143	$r =$ 0.2019		(b)	$A_1 =$ 0.6159	$A_2 =$ 0.00094	$B_1 =$ 0.0463			
1.3	$m =$ 0.8575	$r =$ 0.1978		(b)	$A_1 =$ 0.6146	$A_2 =$ 0.00094	$B_1 =$ 0.0460			
1.4	$m =$ 0.4104	$r =$ 0.2575	$q =$ 0.4376	(b)	$A_1 =$ 0.6360	$A_2 =$ = 0.00094	$B_1 =$ 0.0485			
1.4*	$m =$ 0.4977	$r =$ 0.2462		(b)	$A_1 =$ 0.6328	$A_2 =$ = 0.00094	$B_1 =$ 0.0475			
1.5	$m =$ 0.8573	$r =$ 0.1978	$q =$ 0.0	(b)	$A_1 =$ 0.6146	$A_2 =$ = 0.00094	$B_1 =$ 0.0460			
1.6	$m =$ 0.0280			(b)	$A_1 =$ 0.6316	$A_2 =$ = 0.00091	$B_1 =$ 0.0446			
1.6*	$m =$ 0.5768	$r =$ 0.3062		(b)	$A_1 =$ 0.6364	$A_2 =$ = 0.00095	$B_1 =$ 0.0487			
2.1	$\alpha =$ 0.4496	$\beta =$ 0.9999		(c)	$G_c =$ 0.6617	$G_e =$ = 0.6518	$1/n =$ 0.0193			
2.2	$\alpha =$ 0.1380	$\beta =$ 0.6534		(c)	$G_c =$ 0.5815	$G_e =$ = 0.0494	$1/n =$ 0.0203			
2.3	$\alpha =$ 0.3164	$\beta =$ 0.9999		(a)	$c_{10} =$ 0.3372	$c_{20} =$ = 0.0	$c_{30} =$ 0.00038	$c_{01} =$ 0.0034	$c_{11} =$ 0.0017	
2.4	$\alpha =$ 0.0151	$\beta =$ 0.6282		(c)	$G_c =$ 0.6172	$G_e =$ = 0.0	$1/n =$ 0.0180			
2.4*	$\alpha =$ 0.0151	$\beta =$ 0.6282		(c)	$G_c =$ 0.6172	$G_e =$ = 0.0	$1/n =$ 0.0180			
2.5	$\alpha =$ 0.0126	$\beta =$ 0.4031		(c)	$G_c =$ 0.5984	$G_e =$ = 0.0157	$1/n =$ 0.0188			
2.6	$\alpha =$ 0.1558	$\beta =$ 0.9999		(c)	$G_c =$ 0.6735	$G_e =$ = 0.0	$1/n =$ 0.0174			
3.1a	$\Delta X_0 =$ 2.9250	$X_\infty =$ 1.0326	$\gamma =$ 0.2082	(a)	$c_{10} =$ 0.0868	$c_{20} =$ = 0.00009	$c_{30} =$ 0.00001	$c_{01} =$ 0.0	$c_{11} =$ 0.00001	
3.1b	$\Delta X_0 =$ 3.0986	$X_\infty =$ 1.0164	$\gamma =$ 0.4388	(a)	$c_{10} =$ 0.0880	$c_{20} =$ = 0.00010	$c_{30} =$ 0.00001	$c_{01} =$ 0.0	$c_{11} =$ 0.00002	
3.2	$\chi =$ 3.0899	$\gamma =$ 26.4669		(c)	$G_c =$ 0.3043	$G_e =$ = 0.0237	$1/n =$ 0.0154			
3.2*	$\chi =$ 2.6181	$\gamma =$ 8.1740		(c)	$G_c =$ 0.2224	$G_e =$ = 0.0214	$1/n =$ 0.0053			

Table 6 Units of the fitting parameters

Mod. No.	Parameters and units									
(a)	c_{10}	MPa	c_{20}	MPa	c_{30}	MPa	c_{01}	MPa	c_{11}	MPa
(b)	A_1	MPa	A_2	MPa	B_1	MPa				
(c)	G_c	MPa	G_e	MPa	$1/n$	-				
1.1	c	-	Δb	-	η_{\min}	-				
1.2	m	$\frac{\text{mm}^3}{\text{Nmm}}$	r	-						
1.3	m	$\frac{\text{mm}^3}{\text{Nmm}}$	r	-						
1.4/1.4*	m	$\frac{\text{mm}^3}{\text{Nmm}}$	r	-	q	-				
1.5	m	$\frac{\text{mm}^3}{\text{Nmm}}$	r	-	q	$\frac{\text{mm}^3}{\text{Nmm}}$				
1.6/1.6*	m	$\frac{\text{mm}^3}{\text{Nmm}}$	r	-						
2.1	α	$\frac{\text{mm}^3}{\text{Nmm}}$	β	-						
2.2	α	$\frac{\text{mm}^3}{\text{Nmm}}$	β	-						
2.3	α	-	β	-						
2.4/2.4*	α	-	β	-						
2.5	α	-	β	-						
2.6	α	-	β	-						
3.1a/b	ΔX_0	-	X_∞	-	γ	-				
3.2/3.2*	χ	-	γ	-						

B Fitting results

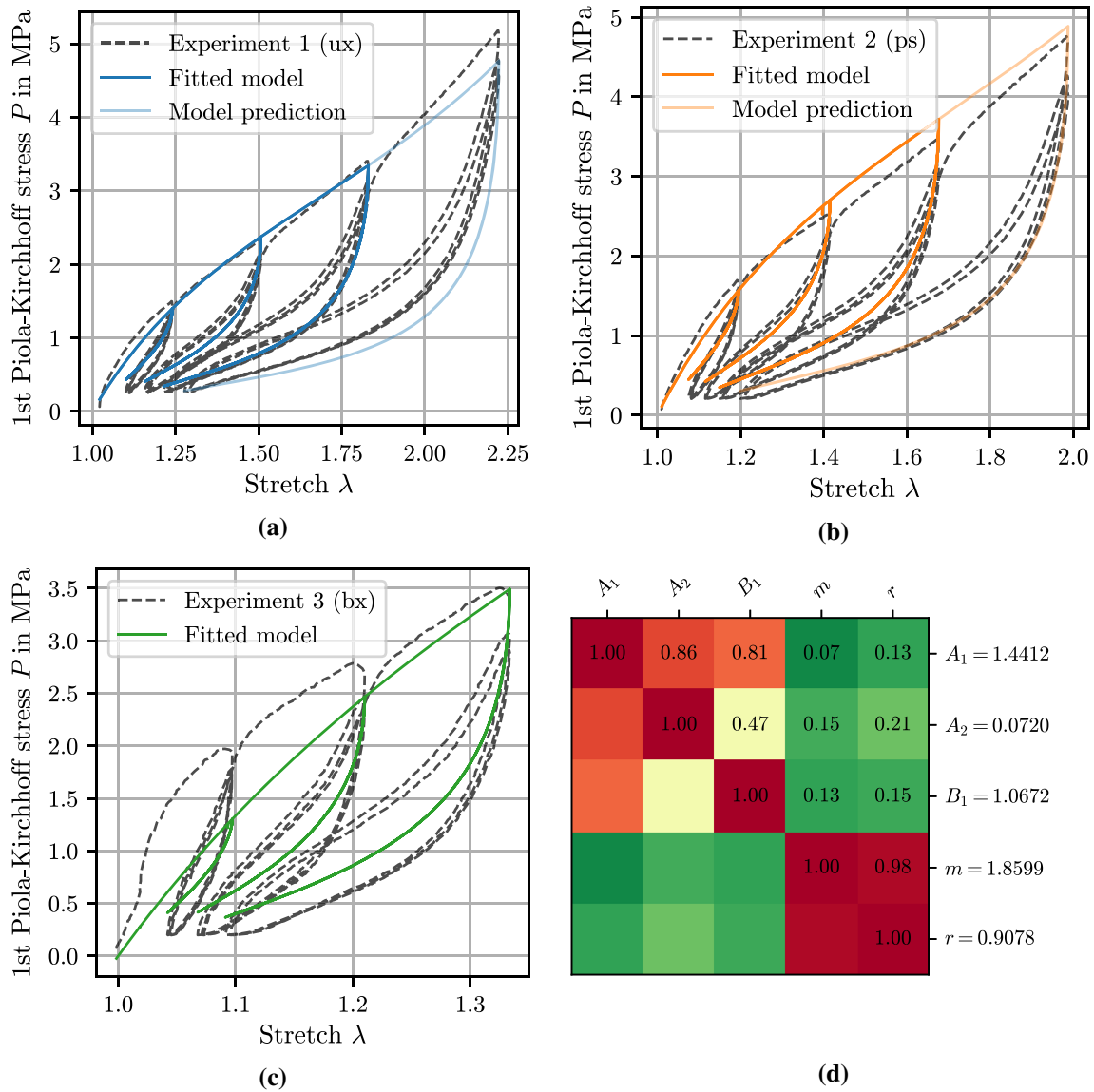


Fig. 8 Fitting results for the stiff compound of the model 1.6* ([15] modified) combined with the strain energy function (b) from [40]: (a-c) Stress vs. stretch for uniaxial, pure shear and equibiaxial loading (the small drop in stress in the virgin load of the pure shear experiment (b) at $\lambda = 1.4$ stems from an outlier in the experimental data), d parameter correlation matrix

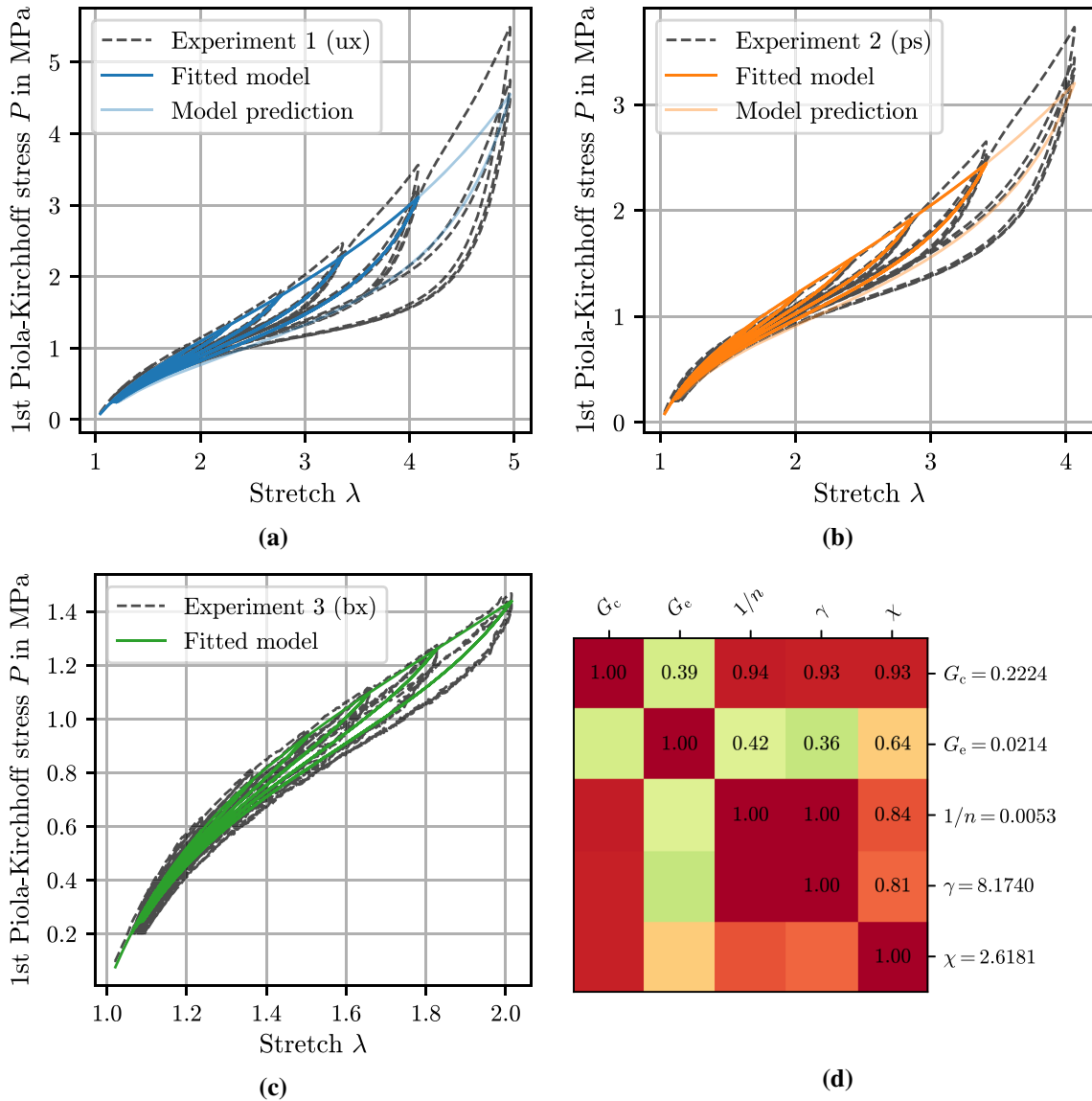


Fig. 9 Fitting results for the soft compound of the model 3.2 by [34] combined with the strain energy function (c) from [35]: (a–c) Stress vs. stretch for uniaxial, pure shear and equibiaxial loading, d parameter correlation matrix

References

- Alexander, H.: A constitutive relation for rubber-like materials. *Int. J. Eng. Sci.* **6**(9), 549–563 (1968). [https://doi.org/10.1016/0020-7225\(68\)90006-2](https://doi.org/10.1016/0020-7225(68)90006-2)
- Beatty, M.F., Krishnaswamy, S.: A theory of stress-softening in incompressible isotropic materials. *J. Mech. Phys. Solids* **48**(9), 1931–1965 (2000). [https://doi.org/10.1016/S0022-5096\(99\)00085-X](https://doi.org/10.1016/S0022-5096(99)00085-X)
- Bergström, J.S., Boyce, M.C.: Mechanical behavior of particle filled elastomers. *Rubber Chem. Technol.* **72**(4), 633–656 (1999). <https://doi.org/10.5254/1.3538823>
- Besdo, D., Ihlemann, J.: A phenomenological constitutive model for rubberlike materials and its numerical applications. *Int. J. Plast.* **19**(7), 1019–1036 (2003). [https://doi.org/10.1016/S0749-6419\(02\)00091-8](https://doi.org/10.1016/S0749-6419(02)00091-8)
- Bose, K., Hurtado, J.A., Snyman, M.F., Mars, W.V., Chen, J.Q.: Modelling of stress softening in filled elastomers. In: Busfield, J., Muhr, A. (eds.) *Proceedings of the ECCMR III*, pp. 223–230. A.A. Balkema Publishers (2003)
- Carleo, F., Barbieri, E., Whear, R., Busfield, J.: Limitations of viscoelastic constitutive models for carbon-black reinforced rubber in medium dynamic strains and medium strain rates. *Polymers* **10**(9), 988 (2018). <https://doi.org/10.3390/polym10090988>
- Carroll, M.M.: A strain energy function for vulcanized rubbers. *J. Elast.* **103**(2), 173–187 (2010). <https://doi.org/10.1007/s10659-010-9279-0>

8. Chagnon, G., Verron, E., Gornet, L., Marckmann, G., Charrier, P.: On the relevance of continuum damage mechanics as applied to the Mullins effect in elastomers. *J. Mech. Phys. Solids* **52**(7), 1627–1650 (2004). <https://doi.org/10.1016/j.jmps.2003.12.006>
9. Coleman, B.D., Noll, W.: The thermodynamics of elastic materials with heat conduction and viscosity. *Arch. Ration. Mech. Anal.* **13**(1), 167–178 (1963). <https://doi.org/10.1007/bf01262690>
10. Dal, H., Badienia, Y., Açıkgöz, K., Denli, F.A.: A comparative study on hyperelastic constitutive models on rubber: State of the art after 2006. In: B. Huneau, J.B. Le Cam, Y. Marco, E. Verron (eds.) *Proceedings of the ECCMR XI*, pp. 239–244. CRC Press (2019)
11. de Souza Neto, E.A., Perić, D., Owen, D.R.J.: A phenomenological three-dimensional rate-independent continuum damage model for highly filled polymers: Formulation and computational aspects. *J. Mech. Phys. Solids* **42**(10), 1533–1550 (1994). [https://doi.org/10.1016/0022-5096\(94\)90086-8](https://doi.org/10.1016/0022-5096(94)90086-8)
12. Diani, J., Fayolle, B., Gilormini, P.: A review on the mullins effect. *Eur. Polym. J.* **45**(3), 601–612 (2009). <https://doi.org/10.1016/j.eurpolymj.2008.11.017>
13. Dorfmann, A., Ogden, R.W.: A pseudo-elastic model for loading, partial unloading and reloading of particle-reinforced rubber. *Int. J. Solids Struct.* **40**(11), 2699–2714 (2003). [https://doi.org/10.1016/s0020-7683\(03\)00089-1](https://doi.org/10.1016/s0020-7683(03)00089-1)
14. Dovì, V.G., Paladino, O., Reverberi, A.P.: Some remarks on the use of the inverse hessian matrix of the likelihood function in the estimation of statistical properties of parameters. *Appl. Math. Lett.* **4**(1), 87–90 (1991). [https://doi.org/10.1016/0893-9659\(91\)90129-j](https://doi.org/10.1016/0893-9659(91)90129-j)
15. Elías-Zúñiga, A.: A phenomenological energy-based model to characterize stress-softening effect in elastomers. *Polymer* **46**(10), 3496–3506 (2005). <https://doi.org/10.1016/j.polymer.2005.02.093>
16. Gehrmann, O., Kröger, N.H., Erren, P., Juhre, D.: Estimation of the compression modulus of a technical rubber via cyclic volumetric compression tests. *Technische Mechanik* **37**(1), 28–36 (2017). <https://doi.org/10.24352/UB.OVGU-2017-048>
17. Gracia, L.A., Peña, E., Royo, J.M., Pelegay, J.L., Calvo, B.: A comparison between pseudo-elastic and damage models for modelling the mullins effect in industrial rubber components. *Mech. Res. Commun.* **36**(7), 769–776 (2009). <https://doi.org/10.1016/j.mechrescom.2009.05.010>
18. Haupt, P.: *Continuum Mechanics and Theory of Materials*, 2nd edn. Springer, Berlin, Heidelberg (2002). <https://doi.org/10.1007/978-3-662-04775-0>
19. Hurtado, J.A., Lapczyk, I., Govindarajan, S.M.: Parallel rheological framework to model non-linear viscoelasticity, permanent set, and mullins effect in elastomers. In: N. Gil-Negrete, A. Alonso (eds.) *Proceedings of the ECCMR VIII*, pp. 95–100. CRC Press (2013)
20. James, A.G., Green, A., Simpson, G.M.: Strain energy functions of rubber I. Characterization of gum vulcanizates. *J. Appl. Polym. Sci.* **19**(7), 2033–2058 (1975). <https://doi.org/10.1002/app.1975.070190723>
21. Kaliske, M., Heinrich, G.: An extended tube-model for rubber elasticity: statistical-mechanical theory and finite element implementation. *Rubber Chem. Technol.* **72**(4), 602–632 (1999). <https://doi.org/10.5254/1.3538822>
22. Kazakevičiūtė-Makovska, R.: Experimentally determined properties of softening functions in pseudo-elastic models of the mullins effect. *Int. J. Solids Struct.* **44**(11–12), 4145–4157 (2007). <https://doi.org/10.1016/j.ijsolstr.2006.11.012>
23. Klüppel, M., Schramm, J.: A generalized tube model of rubber elasticity and stress softening of filler reinforced elastomer systems. *Macromol. Theory Simul.* **9**(9), 742–754 (2000). [10.1002/1521-3919\(20001201\)9:9<742::aid-mats742>3.0.co;2-4](https://doi.org/10.1002/1521-3919(20001201)9:9<742::aid-mats742>3.0.co;2-4)
24. Laiarinandrasana, L., Piques, R., Robisson, A.: Visco-hyperelastic model with internal state variable coupled with discontinuous damage concept under total lagrangian formulation. *Int. J. Plast.* **19**(7), 977–1000 (2003). [https://doi.org/10.1016/s0749-6419\(02\)00089-x](https://doi.org/10.1016/s0749-6419(02)00089-x)
25. Lambert-Diani, J., Rey, C.: New phenomenological behavior laws for rubbers and thermoplastic elastomers. *Eur. J. Mech. A. Solids* **18**(6), 1027–1043 (1999). [https://doi.org/10.1016/s0997-7538\(99\)00147-3](https://doi.org/10.1016/s0997-7538(99)00147-3)
26. Le Cam, J.B.: A review of volume changes in rubbers: the effect of stretching. *Rubber Chem. Technol.* **83**(3), 247–269 (2010). <https://doi.org/10.5254/1.3525684>
27. Lorenz, H., Klüppel, M.: A microstructure-based model of the stress-strain behavior of filled elastomers. In: Heinrich, G., Kaliske, M., Lion, A., Reese, S. (eds.) *Proceedings of the ECCMR VI*, pp. 423–428. CRC Press (2009)
28. Marckmann, G., Verron, E.: Comparison of hyperelastic models for rubber-like materials. *Rubber Chem. Technol.* **79**(5), 835–858 (2006). <https://doi.org/10.5254/1.3547969>
29. Miehe, C.: Discontinuous and continuous damage evolution in Ogden-type large-strain elastic materials. *Eur. J. Mech. A. Solids* **14**(5), 697–720 (1995)
30. Miehe, C., Göktepe, S., Lulei, F.: A micro-macro approach to rubber-like materials - Part I: the non-affine micro-sphere model of rubber elasticity. *J. Mech. Phys. Solids* **52**(11), 2617–2660 (2004). <https://doi.org/10.1016/j.jmps.2004.03.011>
31. Mullins, L., Tobin, N.R.: Stress softening in rubber vulcanizates. part i. use of a strain amplification factor to describe the elastic behavior of filler-reinforced vulcanized rubber. *J. Appl. Polym. Sci.* **9**(9), 2993–3009 (1965). <https://doi.org/10.1002/app.1965.070090906>
32. Naumann, C., Ihlemann, J.: On the thermodynamics of pseudo-elastic material models which reproduce the Mullins effect. *Int. J. Solids Struct.* **69–70**, 360–369 (2015). <https://doi.org/10.1016/j.ijsolstr.2015.05.014>
33. Ogden, R.W., Roxburgh, D.G.: A pseudo-elastic model for the Mullins effect in filled rubber. *Proc. R. Soc. A* **455**(1988), 2861–2877 (1999). <https://doi.org/10.1098/rspa.1999.0431>
34. Plagge, J., Klüppel, M.: A physically based model of stress softening and hysteresis of filled rubber including rate- and temperature dependency. *Int. J. Plast.* **89**, 173–196 (2017). <https://doi.org/10.1016/j.ijplas.2016.11.010>
35. Plagge, J., Ricker, A., Kröger, N.H., Wriggers, P., Klüppel, M.: Efficient modeling of filled rubber assuming stress-induced microscopic restructurization. *Int. J. Eng. Sci.* **151**, 103291 (2020). <https://doi.org/10.1016/j.ijengsci.2020.103291>
36. Raghunath, R., Juhre, D., Klüppel, M.: A physically motivated model for filled elastomers including strain rate and amplitude dependency in finite viscoelasticity. *Int. J. Plast.* **78**, 223–241 (2016). <https://doi.org/10.1016/j.ijplas.2015.11.005>
37. Ricker, A., Fehse, A., Kröger, N.H.: Charakterisierung sowie Modellbildung zur Beschreibung von Kompressionsmoduln technischer Gummierwerkstoffe. Schlussbericht zu IGF-Vorhaben Nr. 19916 N, Deutsches Institut für Kautschuktechnologie e.V. (2020)

38. Simo, J.C.: On a fully three-dimensional finite-strain viscoelastic damage model: Formulation and computational aspects. *Comput. Methods Appl. Mech. Eng.* **60**(2), 153–173 (1987). [https://doi.org/10.1016/0045-7825\(87\)90107-1](https://doi.org/10.1016/0045-7825(87)90107-1)
39. Steinmann, P., Hossain, M., Possart, G.: Hyperelastic models for rubber-like materials: consistent tangent operators and suitability for Treloar's data. *Arch. Appl. Mech.* **82**(9), 1183–1217 (2012). <https://doi.org/10.1007/s00419-012-0610-z>
40. Swanson, S.R.: A constitutive model for high elongation elastic materials. *J. Eng. Mater. Technol.* **107**(2), 110–114 (1985). <https://doi.org/10.1115/1.3225782>
41. Wrubleski, E.G.M., Marczak, R.J.: Modification of hyperelastic incompressible constitutive models to include nonconservative effects. In: *Proceedings of the 22nd COBEM* (2013)
42. Wrubleski, E.G.M., Marczak, R.J.: A study on the inclusion of softening behavior in hyperelastic incompressible constitutive models. In: Marvalová, B., Petriková, I. (eds.) *Proceedings of the ECCMR IX*, pp. 289–296. CRC Press (2015)
43. Yeoh, O.H.: Characterization of elastic properties of carbon-black-filled rubber vulcanizates. *Rubber Chem. Technol.* **63**(5), 792–805 (1990). <https://doi.org/10.5254/1.3538289>

Publisher's Note Springer Nature remains neutral with regard to jurisdictional claims in published maps and institutional affiliations.